



Research article

Composite polymer/wax coatings as a corrosion barrier of bioresorbable magnesium coronary stents

Tonya D. Andreeva^{a,b,*}, Oliver Walker^a, Alexander Rudt^a, Ole Jung^c,
Mike Barbeck^c, Manfred Gülcher^{d,e}, Rumen Krastev^{a,f,**}

^a Faculty "Life Sciences", Reutlingen University, Alteburgstraße 150, 72762, Reutlingen, Germany

^b Institute of Biophysics and Biomedical Engineering, Bulgarian Academy of Sciences, Acad. G. Bonchev Str. 21, 1113, Sofia, Bulgaria

^c Clinic and Policlinic for Dermatology and Venereology, University Medical Center Rostock, Strempelstraße 13, 18057, Rostock, Germany

^d QualiMed Innovative Medizinprodukte GmbH, 21423, Winsen, Germany

^e Subsidiary of Q3 Medical Devices, Ireland

^f Department "Material Development and Functionalization", NMI Natural and Medical Sciences Institute at the University of Tübingen, 72770, Reutlingen, Germany

ARTICLE INFO

Keywords:

Magnesium alloy
Mg-based stents
Corrosion resistance
In-vitro degradation
Composite coatings

ABSTRACT

Magnesium and its alloys are suitable materials for biodegradable biomedical implants such as cardiovascular stents. Here we introduce an innovative composite polyelectrolyte multilayer/wax coating applied to commercial coronary Mg-based stents serving as a barrier layer effectively retarding corrosion. This hydrophobic coating, build by layer-by-layer technology, appeared very thin, smooth, homogeneous, strongly adherent and completely covering the surface of the Mg-stent. *In-vitro* degradation tests showed greater resistance to degradation of coated Mg-stents compared to uncoated and passivated ones. Cytocompatibility studies proved that Mg-stent coated with the composite coating was non-cytotoxic and improved fibroblast cell viability compared to the uncoated Mg-stent.

1. Introduction

Second-generation drug-eluting metal stents (DES) loaded with antiproliferative agents represent the current conventional approach to the treatment of obstructive coronary artery disease. They were designed to address the early (0–30 days) and late (1–12 months) side effects of the bare metal stents and first-generation DES referring to incomplete reendothelialization caused by drug-inhibited neointimal hyperplasia, chronic vessel inflammation and incomplete stent apposition. However, the most comprehensive meta-analysis to date of all published DES data covering more than 31 000 patients cases yielded inconsistent results regarding treatment outcomes [1]. Second- and first-generation DES demonstrated similar short-term and long-term cardiac mortality rates. Yet the odds of myocardial infarction after the implementation of the second-generation DES were 23 % less in the short-term and 50 % less in the long-term when compared to first generation DES. The second-generation everolimus-eluting stent (EES) was found to profoundly reduce the short- and long-term odds of stent thrombosis compared to the first -generation DES, however the second-generation zotarolimus-eluting stent (ZES-E) caused an increase in the thrombosis cases. Regarding revascularization, the

* Corresponding author. Faculty "Life Sciences", Reutlingen University, Alteburgstraße 150, 72762, Reutlingen, Germany.

** Corresponding author. Faculty "Life Sciences", Reutlingen University, Alteburgstraße 150, 72762, Reutlingen, Germany.

E-mail address: tonya.andreeva@reutlingen-university.de (T.D. Andreeva).

<https://doi.org/10.1016/j.heliyon.2024.e34025>

Received 1 May 2024; Received in revised form 20 June 2024; Accepted 2 July 2024

Available online 3 July 2024

2405-8440/© 2024 The Authors. Published by Elsevier Ltd. This is an open access article under the CC BY-NC license (<http://creativecommons.org/licenses/by-nc/4.0/>).

comparison between first- and second-generation DES leads to contradictory outcomes that are related to the specific product and manufacturer. Overall, first- and second-generation DES are considered to have a similar level of efficacy, but the second-generation DES is regarded as increasing the level of safety during application [1]. In terms of the very long-term performance (up to 5 years), no significant reduction in major adverse cardiac events was associated with second-generation compared to first-generation DES [2]. As the possibilities for further optimization of the DES are generally exhausted, currently a great hope is assigned to the application of bioresorbable stents (BRS). BRS are intended to provide temporally support to the acute vessel until the healing process and are subsequently completely resorbed by the body, thus eliminating long term complications caused by the foreign body implant material.

The first bioresorbable coronary stent based on a magnesium alloy was designed in 2003 as a replacement of the permanent DES [3] with the aim to overcome the DES' drawbacks such as late thrombosis and formation of blood clots, local inflammatory reactions, impaired endothelial function. Due to low corrosion resistance magnesium and its alloys emerge as suitable materials for temporal biomedical implants such as cardiovascular stents. When conventional stent materials such as steel remain in the body long after the finalized healing process, they cause long-term side effects. Biosorption of Mg-based stents eliminates the causes for these long-term effects.

On one hand the rapid corrosion of Mg and Mg-alloys is necessary for the biosorption, on the other hand a controlled degradation rate is not easy to accomplish. Chloride-containing environments like body fluids lead to unpredictable and uncontrollable velocities of degradation. If the degradation speed is too high, toxic byproducts overwhelm and irritate the surrounding tissue, if the speed is too low, the temporal implant might not accomplish its purpose of supporting the blood vessel long enough until healing takes place.

The various approaches and materials used for surface modification or coating of Mg-based alloys to slow down and regulate the degradation are impossible to enumerate [4]. Among them, the biocompatible organic coatings obtained by dip-coating or spray-coating of Mg surfaces with a solution of the corresponding organic compound are scarce.

Polymer-based biodegradable coatings have already been shown to regulate the degradation rate and improve the corrosion resistance and biocompatibility of Mg-based substrates by minimizing the release of degradation products. Polymer coatings based on chitosan (CHI) with different molecular weight (from 10 kDa to 600 kDa) and deacetylation degree (from 83 % to 90 %) have been shown to improve the corrosion resistance of 2 mm thick Mg–Ca-alloy discs [5]. Polycaprolactone (PCL) and polylactic acid (PLA) coatings with thickness of 15–20 μm applied by dip-coating have been shown to interact with the surface of high-purity magnesium, thus weakening the corrosion resistance [6]. PCL coating, when spray-coated on MgAlZn-alloy, demonstrated a porous structure with adjustable pore size, thus allowing for regulation of the degradation rate [7]. PLA and poly(desaminotyrosyl tyrosine hexyl carbonate) coatings deposited on 1 mm thick MgAlZn foil by spray-coating induced 5 to 7 times drop of the degradation rate [8]. Application of dip-coated poly(lactide-co-glycolide) (PLGA) coating was reported to decrease the degradation rate of Mg–6Zn-alloy in 0.9 % NaCl by two orders of magnitude [9]. A comparative study of four biodegradable spin-coated polymer coatings (Poly(L-lactide) PLLA, PLGA (90:10), PLGA (50:50), and PCL) revealed that they were all capable of delaying the Mg-degradation, with PLGA (50:50) being the most promising [10]. Mg-discs coated with low- and high-molecular weight PLLA and PCL demonstrated significant retardation of the degradation compared to uncoated discs after 10 days of immersion into degradation solution, with the PLLA coating being more favorable [11]. Another study indicated that between dip-coated PLA, PLGA and PCL coatings, PLA was the one demonstrating the highest biocompatibility, hemocompatibility and corrosion resistance [12].

Polymer coatings constructed by layer-by-layer (LbL) deposition of polyelectrolytes on Mg-alloy substrates also demonstrated a potential for corrosion protection and biocompatibility. The literature data are contradictory and generally show that stand-alone polyelectrolyte multilayers (PEM), being swellable and allowing penetration of the corrosive electrolyte ions, are not highly efficient in protecting the Mg-substrate from degradation. Given the limitations of the stand-alone PEM, composite coatings that combine PEM with one or more additional auxiliary barrier layers have been developed and studied, and they offer significantly improved corrosion protection performance coupled with biocompatibility. The first study reported on the construction of PEM, composed of poly(ethylene imine) (PEI) and poly(styrene sulfonate) (PSS), with 8-hydroxyquinoline (8HQ) embedded between PSS-layers as corrosion inhibitor, on AZ91D-alloy. The PEM was cross-linked with glutaraldehyde and found to be cytocompatible [13]. Electrochemical corrosion tests demonstrated that LbL coatings of the natural polyelectrolytes CHI and pectin have no impact on the degradation behavior of Mg-alloy [14]. Poly-L-lysine PLL/Alginate coating on passivated AZ31 substrates did not improve the *in-vitro* degradation kinetics of the substrate and surprisingly did not promote cell adhesion and growth [15]. PEM modification by EDC-NHS cross-linking and immobilization of fibronectin reduced the cytotoxicity of the coating [15]. The corrosion profiles of AZ31-alloy coated with poly(allylamine hydrochloride) PAH/PLGA(50:50), PAH/PLGA(75:25) and PAH/PCL multilayers revealed reduced corrosion rate compared to the uncoated substrate, accompanied by improved biocompatibility [16]. Polystyrene sulfonate PSS/PAH multilayer capped with polymethyltrimethoxysilane enhanced the corrosion resistance of AZ31-alloy, unlike the PSS/PAH multilayer alone that was damaged in 48 h of degradation [17]. One very recent study showed that a composite coating composed of poly(vinylpyrrolidone) (PVP)/polyacrylic acid (PAA) multilayers shielded with calcium-bearing phosphate (Ca–P) coat had superior corrosion protection of AZ31-alloy than the Ca–P layer alone [18]. Potentiodynamic polarization tests displayed that microarc oxidation coating (MAO), known to strongly reduce the corrosion rate of Mg, only slightly improved the corrosion resistance of WE43-alloy when applied alone, but when associated with a 50-bilayers thick PSS/CHI multilayer increased the resistance 20 times [19]. Application of composite coatings, combining cerium-based conversion layer (Ce) and self-healing PEI/PAA multilayer had no impact on the corrosion resistance of AZ31-alloy, due to the penetration of chloride anions through the PEM [20]. However, incorporation of single nanometer thick graphene oxide (GO) layer between Ce and PEM layers served as a physical barrier hindering the diffusion of electrolytes and improved the corrosion resistance [20]. Significant improvement of the short-term corrosion resistance, biocompatibility and thromboresistance of AZ31B-alloy was achieved by utilization of electrostatically assembled coating of CHI-functionalized GO and heparin [21].

Currently, there are few marketed prototypes of Mg-alloy-based coronary stents that are all still under development, in pre-clinical or post-clinical stage [22], but the concerns about rapid degradation and failure remain. The scaffold of the coronary Mg-stent is extremely fine and the challenge is to build a coating without any defects (holes), capable of providing an effective barrier functionality. Moreover, spray-coating and spin-coating technologies are not applicable as they do not allow coating complex shapes such as coronary stents.

So far, there are only a few studies addressing the utilization of coatings for controlled *in-vitro* and/or *in-vivo* degradation of bioabsorbable vascular stents based on Mg-alloys. First one reports on utilization of a bioresorbable PLGA matrix loaded with the antiproliferative drug paclitaxel on an AMS-3.0 scaffold (Biotronik AG, Switzerland), made of slowly degradable WE43-alloy [23]. Three types of PLGA with different compositions were employed for the construction of the coatings – PLGA(50:50) and PLGA(85:15) with low and high molecular weight. The thickness of the drug-loaded coatings was 3 μm for PLGA(50:50) and 1 μm for both types of PLGA(85:15). The average degradation rates of the three types of PLGA-coated Mg-based AMS-3.0 stents in *in-vivo* conditions were 0.036–0.072 $\text{mg}/(\text{cm}^2 \cdot \text{day})$ [23]. In another study self-made coronary stent prototypes and discs made of the patented Mg-Nd-Zn-Zr alloy (JDBM-stents) were coated with 4–6 μm thick rapamycin-loaded poly(D,L-lactic acid) (PDLLA) coating and subjected to *in-vitro* and *in-vivo* degradation [24]. PDLLA-coated JDBM-stent reveals better preserved structural integrity than Biotronik's DREAMS 1G-stent (Biotronik, Switzerland) but inferior than DREAMS 2G-stent, 3 months after implantation into porcine coronary arteries [24]. A prototype of AZ31-based stent, passivated with 46 % hydrofluoric acid and further spray coated with tetrahydrofuran solution of PDLLA, was found to have enhanced corrosion resistance in an *in-vitro* degradation study compared to a bare Mg-alloy stent [25]. Other self-made Mg-stent prototypes made of AZ31 Mg-alloy and dip-coated with poly(carbonate urethane) urea showed superior corrosion retardation than PLGA (50:50) coated and uncoated stents [26]. According to a very recent *in-vivo* study in pig and rabbit models, a 100 μm thick electrospun biodegradable coating of L-Lactide- ϵ -caprolactone-trimethylene carbonate-glycolide on Mg-based stent backbone has shown better performance than the same coating fabricated by dip-coating [27]. Sequential spray-coating of WE43 stent with a sirolimus-eluting polymer coating, that was asymmetric with respect to the luminal (coated with PEI layer) and abluminal (coated with PLGA/PEI bilayer) surfaces demonstrated a great improvement in stent corrosion resistance [28]. In other study, a protein coating (silk fibroin with sirolimus) was applied on a Mg-alloy (AZ31) stent and its superiority over the conventional biodegradable PDLLA and PCL coatings was revealed under *in-vitro* degradation conditions [29].

This study reports on the construction of a composite biocompatible coating, based on polyelectrolyte multilayers and wax, which is much thinner than the polymer coatings previously studied, but being hydrophobic it forms a waterproof barrier layer protecting the Mg-alloy from contact with the aqueous environment. The proposed coating was applied to commercial bioresorbable Mg-stents by layer-by-layer technology and proved to be very effective in protecting the stents from rapid degradation. Three types of wax particles and an advanced coating approach were applied to modify the surface of Mg-stents and to enhance the corrosion resistance. Integrity loss, mass loss, mechanical stability loss as well as morphology changes have been used to assess and compare the corrosion rate of uncoated and coated biodegradable Mg-stents in *in-vitro* tests. Furthermore, the cytotoxicity of the coatings was studied.

2. Materials and methods

2.1. Materials

Polyelectrolytes - poly(ethylene imine) (PEI, 750 kDa) and polystyrene sulfonate (PSS, 70 kDa), both from Sigma Aldrich (Steinheim, Germany), and poly(allylamine hydrochloride) (PAH, 120–200 kDa) from Alfa Aesar (Thermo Fisher (Kandel) GmbH) were all used as received. PSS and PAH were both dissolved in 0.5 M NaCl to a concentration of 2 mg/ml and adjusted to pH 7.0. PEI was dissolved in ultrapure water to a concentration of 2 mg/ml and adjusted to pH 7.0. The three aqueous wax suspensions (25–50 % w/w), named here W1, W2 and W3, two with anionic and one with cationic particles, were purchased from Keim *additec* Surface GmbH. The wax particles were paraffin-based, with spherical shape. The melting ranges (as listed by the supplier) and diameter and zeta-potential (as measured with dynamic light scattering) are listed in Table 1. Because Mg-stents break down very fast upon contact with watery solutions, wax particles were resuspended in ethanol to a final concentration of 3 % w/w.

2.2. Preparation of composite PEM/wax coatings

Silicon (100) wafers (10 mm \times 10 mm, CrysTec GmbH, Germany) and Mg-stents (length 17 mm, diameter 4 mm) were used as tests samples. Si-wafers were preliminary cleaned by consecutive ultrasonication in acetone and isopropanol (2 min each) and activated by oxygen plasma cleaning. Mg-stents were provided from QualiMed Innovative Medizinprodukte GmbH, Germany (subsidiary of Q3 Medical Devices, Ireland). The stents were machined from a magnesium alloy containing two alloying elements, one of which was a

Table 1
Characteristic parameters of the three types of wax-particles applied for construction of the barrier-layers.

Parameter	Wax type		
	W1	W2	W3
Melting range, °C	~56–58	~56–85	~46–58
Diameter, nm	170.6 \pm 1.9	65.2 \pm 0.5	176.0 \pm 1.0
Zeta-potential, mV	–30.4 \pm 1.9	–44.8 \pm 2.9	+59.4 \pm 1.8

rare earth element. Mg-stents were used without pretreatment. The coating was preceded by passivation intended to protect the stents from initial degradation during incubation in polyelectrolyte solutions. This step was performed following the protocol of Ostrowski et al. [16] by treatment with preheated 5 M NaOH for 2 h at 60 °C. During this treatment, a homogeneous surface layer of Mg(OH)₂ was synthesized, which is poorly soluble in water and therefore protects the underlying Mg-alloy from contact with water in the short term. After the passivation, the stents were rinsed with water 6 times for 10 s each.

PEM were constructed by LbL technique using the hand dipping method described in Ref. [30]. Polycation PAH and polyanion PSS were sequentially adsorbed on the surface, by immersion in the polyelectrolyte solutions. The number of the PSS/PAH bilayers was either 7.0 or 7.5 according to the charge of the wax employed. Cationic wax-particles were adsorbed on PEM with anionic outermost PE layer and vice versa. PEI was used as adhering layer of the PEM to the coated surfaces. This procedure has already shown the formation of a stable PEM on model Si-wafer surfaces [30]. The composition of studied PEM/wax coatings with their abbreviations are listed in Table 2.

Coatings were composed of two building blocks, as shown in Fig. 1. Each building block consisted of PEM, which was hydrophilic and a barrier wax-layer that was hydrophobic and water-repellent. Three types of wax-particles (W1, W2 and W3) with different charge (cationic or anionic) and size (Table 1) were utilized for building of the barrier layer. Wax-layer was created by adsorption of single layer of wax-particles from ethanol suspension, followed by washing with water and annealing during which particles melt and merge, creating a continuous layer. The annealing was conducted by insertion of the coated substrates in a preheated oven for 45 min. The oven temperature was set above the specific melting temperature of the wax type (Table 1). The temperature was set to 60 °C for W1 and W3, and to 90 °C for W2.

2.3. Ellipsometry

The thickness of the PEM on Si-wafers was monitored by spectroscopic ellipsometer SE800 (Sentech Instruments GmbH, Germany) with wavelength range from 280 to 850 nm, at an angle of incidence of 70°. The raw data were fitted by a four-layer model considering the contribution of air (n_D of 1.000), PEM coating (variable n_D), SiO₂ (n_D of 1.5302), and Si (n_D of 3.8858). The measurements were performed in triplicate at five different locations on each sample.

2.4. Static water contact angle

Static contact angles were measured by the sessile drop method using EasyDrop goniometer (Kruss, Germany) equipped with video capture. A drop of 2 µL ultrapure water was placed on the leveled surface of the sample by microsyringe to form a single sessile drop. The left and right contact angles were determined at 5 different spots for each sample by applying the Young-Laplace-fitting of the profile.

2.5. Scanning electron microscopy

Scanning electron microscopy was performed on a DSM 962 field-emission instrument (Zeiss, Germany). High vacuum mode was used with 5–15 kV acceleration voltage. All samples were sputter-coated with 2 nm thin gold layer before the surface morphology observation.

2.6. In-vitro degradation

The degradation tests were performed according to DIN EN ISO 13781 in heat-sterilized Sørensen buffer adjusted to pH 7.4 ± 0.2 as a degradation medium (DM). In compliance with the ISO norm the buffer was prepared by dissolving 1/15 mol/L KH₂PO₄ and 1/15 mol/L Na₂HPO₄ in 1 L of water. The samples were placed each in a separate glass container without any stress. They were fully covered by 500 ml of DM. The high volume of DM was necessary to prevent the pH-elevation accompanying the degradation. The containers were tightly closed to avoid evaporation of the medium and kept into an incubator at 37 °C under continuous shaking at 60 rpm. The pH-value of the medium was monitored before and after the degradation and no change was noted. After 7 days, the stents were washed with water, dried and analyzed.

Table 2
Composition of studied PEM/wax coatings with the abbreviations used in this paper.

COATING	ABBREVIATION
PEI/(PSS/PAH) _{7.0} /W1	PEM/W1
PEI/(PSS/PAH) _{7.0} /W2	PEM/W2
PEI/(PSS/PAH) _{7.5} /W3	PEM/W3
PEI/(PSS/PAH) _{7.0} /W1/(PSS/PAH) _{7.0} /W1	(PEM/W1) ₂
PEI/(PSS/PAH) _{7.0} /W2/(PSS/PAH) _{7.0} /W2	(PEM/W2) ₂
PEI/(PSS/PAH) _{7.5} /W3/(PSS/PAH) _{7.5} /W3	(PEM/W3) ₂

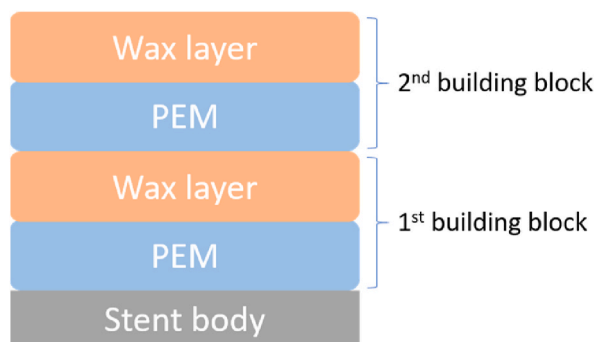


Fig. 1. Scheme of the composite PEM/wax coatings comprising two building-blocks.

2.7. Quantification of the degradation by gravimetric measurements

The relative mass loss of Mg-stents during degradation was detected according to ASTM standards G1 and F1635 and quantified by the formula:

$$\text{Mass Loss \%} = \frac{m_0 - m_t}{m_0} \cdot 100$$

where m_0 was the mass before degradation and m_t was the mass after degradation.

2.8. Quantification of the degradation by integrity determination

All samples were photographically documented at defined reproducible perspective and illumination before coating, after coating - in dry state, and after the degradation - in dry state.

2.9. Quantification of the degradation by crush test

The mechanical crush test quantified the deformation resistance of Mg-stent pressed with a 90 mm diameter stamp. The test was performed according to the ISO 25539-2 and was used to follow the degradation process of the stents according to ISO 13781. The test determined the maximal force (F_{\max}) required to cause a deformation of 50 % corresponding to the diameter reduction. The purpose was to identify the extent to which the stent regained its original mechanical stability after degradation. The examined stent was placed on the lower punch and approached with the upper punch with a pre-force of 5 mN and a speed of 2.5 mm/min. Thus, the initial diameter of the stent was detected. The speed during the deformation was set to 3 mm/min. After reaching 50 % deformation, the stent was released as the upper punch was detached. The resilience of the stent was estimated from the maximal force applied for the deformation.

2.10. In-vitro cytotoxicity assay

The experiments were carried out in triplicate in sterile and aseptic conditions (ISO 10993-5). Necessary controls for positive (cytotoxic latex) and negative (non-cytotoxic polypropylene PP) signals were tested as well (in accordance with ISO 10993-5). The extraction procedure complies with the *in-vivo* conditions for implantation (ISO 10993-5). Samples preparation is described in detail in ISO 10993-12. For the cytotoxicity analysis, an extraction of potentially cytotoxic substances from bare Mg-stents, passivated Mg-stents, Mg-stents coated with (PEM/W2)₂ coating, and controls was carried out. The extraction medium (EM) used was Dulbecco's Modified Eagle Medium (DMEM) with a protein content of 10 % (v/v) FCS (Fetal Calf Serum) (ISO 10993-12). According to ISO 10993-12, the volumes of the EM were adapted to the sample weight and volume. Test bodies (latex, PP, Mg-stents) in small reaction vessels were covered with a volume of 500 μ L DMEM and the extraction was carried out at 37 °C for 24 h in agitation (ISO 10993-5). The extracts were not stored but immediately used for further biological tests.

According to ISO 10993-5, liquid samples such as extracts can be analyzed using well-established cell lines. The cell line used here was L929 and the cell culture medium was DMEM +10 % FCS +1 % penicillin/streptomycin (Gibco, US). The EM was added onto a sub-confluent cell layer. For this purpose, L929 cells were cultivated in cell culture plates for 24 h, the old medium was discarded and replaced with EM. As suggested in ISO 10993-5, a series of dilutions of EM with fresh medium was prepared and tested. After an incubation time of 24 h, the vitality of the surviving cells was tested using the resazurin reduction assay.

When the extracts of studied samples and reference materials (positive and negative control) were evaluated in parallel, the degree of growth inhibition reflects the relative cytotoxicity of the samples. The following relationship was used to estimate the toxicity (here G.I. - Growth Inhibition):

$$G.I. \text{ in } \% = \frac{A_{570}(\text{sample} - \text{blank}) - A_{570}(\text{negative control} - \text{blank})}{A_{570}(\text{positive control} - \text{blank}) - A_{570}(\text{negative control} - \text{blank})} \cdot 100$$

A_{570} (blank) is the absorption of resazurin solution at 570 nm after incubation in wells without cells; A_{570} (sample) is the absorption of resazurin solution after incubation with cells pretreated with EM for 24 h; A_{570} (negative control) is the absorption of resazurin solution after incubation with cells pretreated for 24 h with 100 % (v/v) EM from the negative control (non-cytotoxic PP); A_{570} (positive control) is the absorption of resazurin solution after incubation with cells pretreated for 24 h with 100 % (v/v) EM from the positive control (cytotoxic latex).

2.11. Cell vitality assay

Human umbilical vein endothelial cells (HUVEC) were cultured in T75 tissue culture flasks (Greiner Bio-One GmbH) in endothelial cell growth medium (PromoCell, Germany) at 37 °C in 5 % CO₂ with an initial concentration of 5000 cells/cm².

For the cell adhesion and cell proliferation tests, the PEM- and PEM/Wax-coated tissue culture treated polystyrene wells, TCP (Greiner Bio-One GmbH) were seeded with 50 000 cells/mL and incubated at 37 °C (5 % CO₂) for 24 h and 72 h correspondingly. An uncoated TCP plate was used as a positive control and an uncoated polystyrene well plate (Greiner Bio-One, Germany) was used as a negative control. For assessing the cell viability, a resazurin assay was applied which enables quantification of the cells with well-functioning metabolism. After cell cultivation for 24 h or 72 h the cell culture medium was replaced with a medium containing 10 % resazurin (Sigma-Aldrich GmbH) and incubated for 3 h at 37 °C. In that time, cells metabolized and reduced the resazurin to resorufin, resulting in a color change from blue to fluorescent violet. Absorbance at 574 nm (corresponding to resazurin) and 604 nm (corresponding to resorufin) was measured using a microtiter plate reader (Safire II-Basic, Tecan Austria GmbH).

3. Results and discussion

3.1. Characterization of the composite PEM/Wax coatings prepared on Si-wafers

The composite coatings were built by electrostatic LbL assembly of anionic (PSS) and cationic (PAH) polyelectrolytes and wax-particles. Due to the high charge density at neutral pH PSS and PAH interact strongly and create thin, non-diffusive linear growing PSS/PAH multilayers [31]. Besides, PSS and PAH build pH-responsive PEM that undergo reversible swelling tuned by pH changes [32]. These polyelectrolytes have been studied for applications such as drug delivery systems [33], antimicrobial coatings [34] and platforms for tissue engineering and tissue repair [35]. Adhesion and proliferation of fibroblasts [36], endothelial [37] and osteoblastic cells [38] has been found to be very good on PSS/PAH films. An *in-vivo* study demonstrated that human umbilical arteries coated with PSS/PAH multilayers and implanted in rabbits showed high graft patency without inflammation up to 3 months after the implantation [39].

To prove the successful building of the composite PEM/Wax coatings we examined the thickness and the contact angles after deposition of the PEM film, as well as after the complete construction of the first and the second building block with surface exposed wax-layers (Fig. 2). All three types of wax formed successful coatings as evidenced by the gradual increase in thickness with successive construction of coatings. The base PEM layer, (PSS/PAH)₇, had a thickness of 23.1 ± 2.4 nm, which matched well the literature data [40,41]. The thickness of the first wax-layer built on top of the PEM was 125.7 nm for W1, 81.8 nm for W2 and 177.4 nm for W3 wax. This difference was attributed to the different size of the wax-particles adhered at the PEM surface (Table 1) which, after melting and fusion, produced layers with various thickness. The smallest particles of W2-type produced the thinnest wax-layer and vice versa. The thickness of the wax-layers proved that a continuous array of densely packed wax-particles was adsorbed on the PEM-surface. Compared to the previously published data [40] the thickness of the first W1-layer was 5.2 times higher (125.7 nm here vs. only 24 nm in ref. 40), although the deposition time was shortened (10 min here, compared to 15 min in ref. 40). The reason lies in the utilization of ethanol - instead of water-based suspensions, promoting the adhesion of wax-particles. Ethanol molecules did not affect the affinity of the wax-particles to the PEM-coated surface, but reduced the repulsive potential between the charged wax-particles, thus

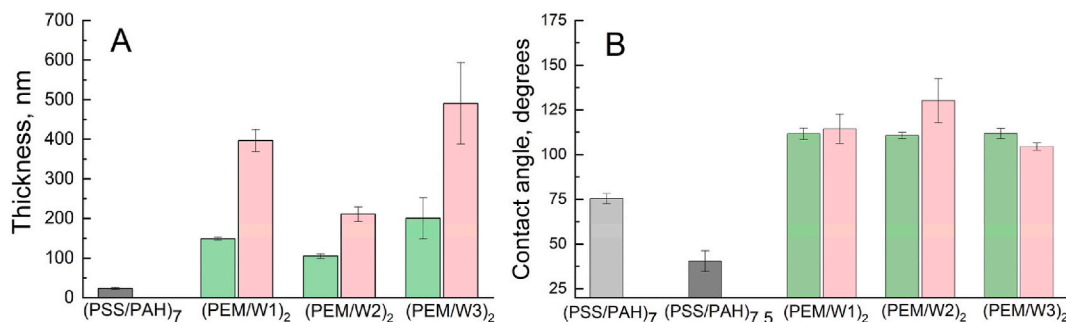


Fig. 2. A) Thickness and B) water contact angle of PEM coating without wax (gray) and with different types of waxes, comprising one (green) or two (red) building blocks.

supporting their agglomeration and faster surface sedimentation [42].

The stepwise growth of the ellipsometric thickness verified the successful adsorption of the charged wax-particles on the oppositely charged PEM surface and of the PEM chains on the continuous wax-layer. The thickness of the second building block was equal to the one of the first in the case of W2 and higher by a factor of 1.7 for W1 and 1.4 for W3 (Fig. 2A). The PEM/W3 coating demonstrated a high deviation in thickness (reaching 20–25 % of the average value), measured after both the first and the second building block. It is worth noting that the deviations were small within a single sample, but large between the three samples examined, so the reason was not attributed to the inhomogeneity of the coatings, but to the reduced build-up reproducibility between the samples.

The PEM films were hydrophilic with static water contact angle of $75 \pm 3^\circ$ for (PSS/PAH)₇ and $41 \pm 6^\circ$ for (PSS/PAH)_{7,5}, but turn into hydrophobic after the deposition of the first wax-layer (Fig. 2B). These data corresponded very well to the previous data, reporting that PSS/PAH coatings with surface exposed PSS-layer were super-hydrophilic, with water contact angle about $20\text{--}40^\circ$, contact angle being dependent on the properties of the substrate, as opposed to the PAH-terminated films which were less hydrophilic, with water contact angles about $60\text{--}80^\circ$ [43]. All coatings comprising one building block demonstrated identical hydrophobicity (contact angle $111 \pm 1^\circ$, agrees well with the data in ref. 40) regardless the type of the wax applied. The hydrophobicity of the second building block resembled the one of the first when W1 or W3 were used and was slightly higher when W2 was used.

The coatings with the three types of waxes had homogeneous morphology, without any defects (surface openings) as identified by SEM (Fig. 3). They adhered very well and completely covered the surface of the substrate. The small round grainy-structures randomly distributed on the surface were the solid crystallization seeds of the commercial wax-particles.

3.2. Coating of Mg-stents and evaluation of degradation resistance

In-vitro corrosion of Mg and Mg-alloys is greatly influenced by experimental parameters such as composition of the degradation medium, dynamic or static conditions, surrounding pH-value and temperature. Therefore, fully simulating the *in-vivo* conditions present in the human body in laboratory studies is still a challenge. Although big variety of liquids have already been utilized as degradation medium, there is no consensus on which best corresponds to the real *in-vivo* conditions. Comparison between the published data about corrosion rate of Mg-alloys is hindered by the extreme sensitivity to the buffer applied and the type and concentration of the electrolytes [44]. The corrosion tests implemented in this study were designed to deliver a consistent and complementary assessment of the protective ability of composite PEM/Wax coatings on Mg-stents.

Taking images of the Mg-stents at each experimental stage is an important tool to detect a possible breakage of the thin strut-connectors, which keep the integrity of the stents but in turn are the weakest structural points and are exposed to the highest wall shear stress caused by the blood flow [45]. Images presented in Table 3 demonstrate that after 7 days of immersion in the degradation medium, untreated and only passivated Mg-stents were highly degraded and only about 1/3 of the stent body volume remained, the rest being completely degraded and dissolved. Studies have shown that the passivation with Mg(OH)₂ coating, although providing a short-term initial protection, breaks down fast in electrolytic solutions, such as the one used in this work, due to its high porosity, roughness and hydrophilicity [16,46]. All coated stents had intact scaffolds after degradation; no segments of stent body were missing.

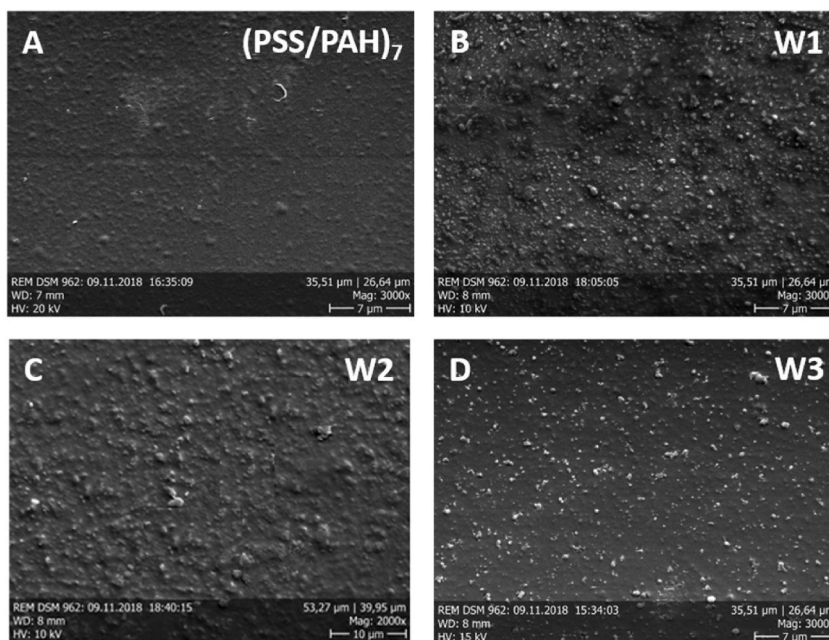



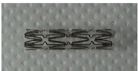

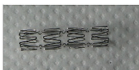













Fig. 3. SEM images of the PEM coating (A) and composite PEM/Wax coatings with two building blocks prepared with wax-particles W1 (B); W2 (C); and W3 (D).

Table 3

Representative images of untreated Mg-stents, passivated Mg-stents, Mg-stents coated with PEM/Wax coatings, and Mg-stents subjected to *in-vitro* degradation.

	Before coating	After passivation	After coating	After degradation
untreated Mg-stent		n.a.	n.a.	
passivated Mg-stent			n.a.	
Mg-stent coated with (sPEM/W1) ₂				
Mg-stent coated with (sPEM/W2) ₂				
Mg-stent coated with (sPEM/W3) ₂				

However, after the exposure to the degradation medium, the Mg-stents coated with (PEM/W1)₂ and (PEM/W3)₂ had thinned bodies as well as 1 or 2 broken strut connectors.

The weight of the untreated Mg-stents amounts to 17.1 ± 0.2 mg and was slightly increased to 17.2 ± 0.2 mg by the passivation (Fig. 4A). The weight of the coated Mg-stents was as follows 17.0 ± 0.2 mg when W1 was used, 17.2 ± 0.2 mg for W2 and 17.1 ± 0.2 mg for W3. After one week of degradation, both the untreated and the passivated Mg-stents lost more than 2/3 of their weight reaching 4.7 mg vs. 5.0 mg respectively. All coated stents demonstrated greater resistance to degradation than the uncoated and passivated stents. The effectiveness of coatings for protection against degradation increased in the following order from least to best protection: (PEM/W3)₂ < (PEM/W1)₂ < (PEM/W2)₂.

The average degradation rates derived from the data in Fig. 4A were as follows: 1.74 mg/day for the bare Mg-stent; 1.79 mg/day for the passivated Mg-stent; 0.66 mg/day for the Mg-stent coated with (PEM/W1)₂; 0.36 mg/day for the Mg-stent coated with (PEM/W2)₂; and 1.11 mg/day for the Mg-stent coated with (PEM/W3)₂. The coating built of W2-wax slowed down the degradation rate 4.8 times compared to the uncoated and passivated Mg-stents thus demonstrating the best degradation protection with only 4 % weight loss in one week.

The maximal force (F_{max}) applied for 50 % deformation of the Mg-stents was as follows: untreated 0.919 N, passivated 0.907 N, coated with (PEM/W1)₂ 0.894 N, coated with (PEM/W2)₂ 0.945 N, and coated with (PEM/W3)₂ 0.863 N (Fig. 4B). After the degradation, testing of the untreated and passivated stent was not feasible because the stents lost their integrity. The results of the crush test showed that (PEM/W2)₂ coating stabilized and supported the scaffold of the Mg-stent thus increasing F_{max} by 5.7 %. Our conclusion was that W2-wax created a barrier layer superior to that of W1- and W3-waxes, which protected the Mg-stents from degradation taking place during PEM build-up, at the contact with the aqueous PE-solutions. Tracking of the data about the weight of the Mg-stents supported this suggestion, since the mass of Mg-stents did not change during the build-up of (PEM/W2)₂ coating, but slightly decreased for (PEM/W1)₂ and (PEM/W3)₂. After the degradation test, the stents coated with (PEM/W2)₂ coating showed

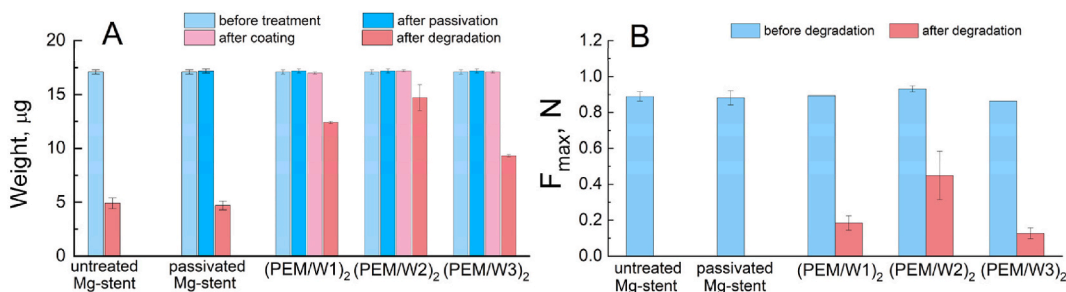


Fig. 4. A) Weights of the untreated Mg-stents, passivated Mg-stents and the Mg-stents coated with the different types of wax, each at different stages of the treatment. B) Maximal force applied for 50 % deformation of the untreated Mg-stents, passivated Mg-stents and Mg-stents coated with the different types of wax, measured before (blue) and after (red) the degradation test. Untreated and passivated Mg-stents were destroyed after the degradation and did not allow the testing.

superior stability against deformation. The efficiency of coatings in protection against degradation, estimated based on the crush test, was found to increase in the line $(\text{PEM}/\text{W}3)_2 < (\text{PEM}/\text{W}1)_2 < (\text{PEM}/\text{W}2)_2$ and was fully consistent with the mass loss findings, namely, the less mass lost, the higher the deformation resistance of the stents.

We hypothesize several reasons why the composite PEM/W2 coating with the thinnest wax-layer displays the best degradation retardation behavior. The efficiency of the coatings in protecting the Mg-stents from degradation, ranked slightly above, increases in the same order as the melting temperature of the wax particles used and is highest for W2 (Table 1). As the *in-vitro* degradation tests were performed at 37 °C, it is possible that some extent of softening or even local melting of the extremely thin wax-layers may occur, which may locally compromise the integrity of the coating. We are not aware of the total composition of the commercial wax particles used in our study, but we observed that both types of negatively charged particles performed better than the positively charged, and the W2 type, which had a stronger negative charge, performed better (Table 1). We assume that the negatively charged particles contain carboxyl-groups that interact strongly with the amino-groups of PAH and thermal cross-linking between the wax-layer and the surrounding PAH layers takes place during the annealing process, resulting in the formation of amide bounds. Heat-induced cross-linking and amide formation were found to increase the stability and decrease the permeability of PEM films containing carboxyl and amine groups [47].

The surfaces of the coated and uncoated Mg-stents before and after the degradation test were examined with SEM to obtain a more in-depth understanding of the coating quality and the degree of degradation. The representative images are presented in Fig. 5. The untreated Mg-stent displayed smooth glossy surface (Fig. 5A1). After the degradation test about 2/3 of the stent body was thoroughly disintegrated and the remaining part was heavily cracked. In the background, multiple pieces of corrosion products detached from the stent body were visible (Fig. 5A2).

The passivation creates a thin solid surface layer of $\text{Mg}(\text{OH})_2$, accordingly the surface of the passivated Mg-stent appeared more rough and less glossy than the one of the untreated Mg-stent (Fig. 5B1). Despite this passivation layer, after 7 days in degradation medium the passivated stent exhibited the same extent of degradation as the unpassivated. About 2/3 of the stent body was crumbled and the remaining part was deeply cracked. The passivation layer was also severely cracked and peeled off from the stent body (Fig. 5B2).

The entire surfaces of the coated Mg-stents were covered by PEM/Wax barrier layers, appearing homogeneous and smooth (Fig. 5C1,D1,E1). Occasionally unmelted wax-particles were seen, suggesting that the annealing step could be prolonged.

After the degradation, the surface of the Mg-stent coated with $(\text{PEM}/\text{W}1)_2$ was evenly cracked, but the cracks were shallow and the whole coating was still intact (Fig. 5C2). The Mg-stent coated with $(\text{PEM}/\text{W}2)_2$ displayed the most shallow cracks and the whole integrity of the coating and the stent was kept (Fig. 5D2). The stent coated with $(\text{PEM}/\text{W}3)_2$ showed many deep cracks and part of the coating was stripped away (Fig. 5E2).

SEM images confirmed the tendency drawn from the gravimetric analysis and the crush test, that the degradation protection of the coatings with different types of wax-particles increased in line: $(\text{PEM}/\text{W}3)_2 < (\text{PEM}/\text{W}1)_2 < (\text{PEM}/\text{W}2)_2$. The surface morphology of the Mg-stents after the degradation test clearly demonstrated the superior degradation protection of $(\text{PEM}/\text{W}1)_2$ and $(\text{PEM}/\text{W}2)_2$ coatings over the PLA and PCL coatings studied before [6]. Although much thicker (15–20 μm) PLA and PCL coatings showed very fractured morphology with many deposits after 8–10 days subjection to degradation [6].

An important question is to what extent the *in-vitro* findings can be extrapolated to a realistic *in-vivo* scenario. Currently, the studies on the *in-vivo* behavior of Mg-alloys and such comparing the degradation rate of Mg-alloys *in-vitro* and *in-vivo* are limited. Our results summarized in Figs. 4 and 5 and in Table 3 show faster degradation of the non-coated stents compared to those which were PEM/Wax coated. Based on the available data, it was estimated that the corrosion rate *in-vivo* was 1–5 times lower than the corrosion rate *in-vitro* [48]. This difference was attributed to the type and concentration of electrolytes used for the *in-vitro* studies [49], in particular the chloride concentration, which was much higher in the degradation media compared to that in the blood plasma. The presence of

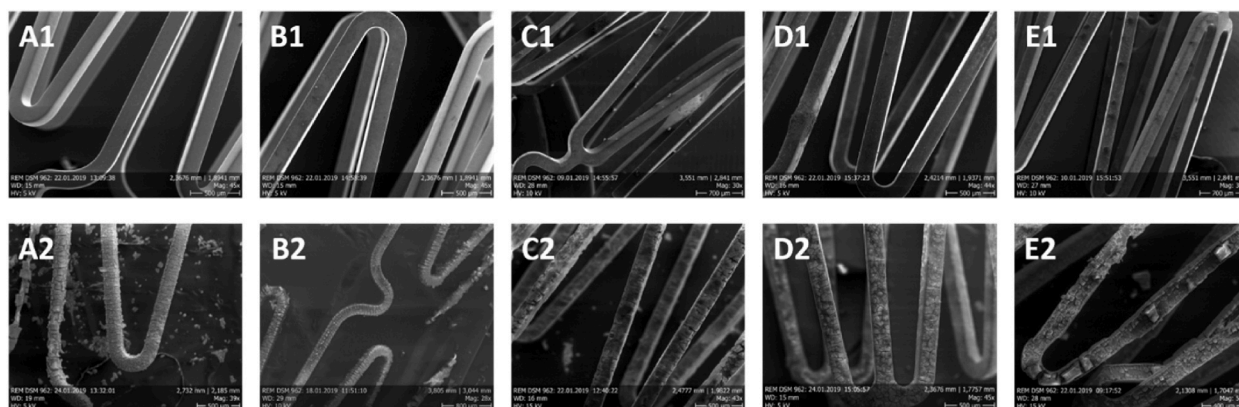


Fig. 5. SEM images of the Mg-stents before (upper row) and after (bottom row) subjection to degradation; (A1 and A2) untreated Mg-stent, (B1 and B2) passivated Mg-stent, (C1 and C2) Mg-stent with $(\text{PEM}/\text{W}1)_2$ coating, (D1 and D2) Mg-stent with $(\text{PEM}/\text{W}2)_2$ coating, (E1 and E2) Mg-stent with $(\text{PEM}/\text{W}3)_2$ coating.

proteins and cells, the location of the implant into the body, as well as the implant-tissue interaction, also contribute to reducing the diffusion rate of electrolytes to the implant surface in *in-vivo* conditions [48].

3.3. Coating of Mg-stents and evaluation of cytotoxicity

The establishment of biocompatibility of medical devices and their constituent components and materials is of great importance to ensure the safety of medical products. This study examined the biocompatibility of overall system including Mg-stent and PEM/Wax coating, according to the standard DIN EN ISO 10993–5 as growth inhibition test with L929 mouse fibroblasts. The DIN EN ISO 10993–5 offers three variations of the cytotoxicity assay – growth inhibition test by direct contact, by indirect contact and by an extract. The latter assesses the presence of extractable cytotoxic substances of medical devices and the results are consistent with those of the animal toxicity tests, since the growth rate of mammalian cells is substantially inhibited in contact with toxic substances.

The conducted cytotoxicity study examined the potential cytotoxic effect of untreated Mg-stents, passivated Mg-stents and Mg-stents coated with our most promising (PEM/W2)₂ coating. The resazurin assay was applied here for quantitative estimation of living cells by assessing their metabolic activity. Fig. 6 shows the growth inhibition of L929 cell line exposed to a dilution series of extracts from untreated, passivated and coated Mg-stents, as well as positive (cytotoxic latex) and negative (non-cytotoxic PP) controls. Controls showed as expected: 100 % cell mortality by the cytotoxic latex at high concentrations, decreasing upon dilution and 0 % cell mortality by the non-cytotoxic PP. Uncoated Mg-stents also revealed strong cytotoxicity at 100 % EM concentration, which was dose dependent and dropped down to 0 % at 50 % EM concentration. L929 mortality was increased by about 18 % when they were exposed to 100 % concentration of EM from the passivated stents and dropped to 0 % at lower concentrations. This proved that the passivation Mg(OH)₂ layer was effective in preventing of Mg-stents from degradation within the first 24 h of incubation. According to ISO 10993–5 if the highest concentration of the sample extract reduces the cell viability with 30 % or less, then the material is considered non-cytotoxic. This *in-vitro* setup displays a static reaction of cells to extracted cytotoxic substances. It needs to be outlined that in *in-vivo* conditions the concentration gradient is steadily decreased by diffusion into surrounding tissue and biological neutralization reactions. It can be assumed that the real dynamic EM concentration gradient in human body would be decreased and cytotoxicity would be reduced in comparison to the *in-vitro* setup.

Cytocompatibility studies proved that coating of Mg-surface with PEM/Wax coating improved the viability of fibroblast cells. Mg-stents coated with the hybrid PEM/W2 coating displayed a cytotoxicity comparable to that of the passivated stents, therefore the PEM coating did not increase the cytotoxicity. Based upon the results in Fig. 6 PEM/W2 coating was considered to not exerting growth-inhibiting effect on L929 mouse fibroblasts.

Because past studies have proved the critical role of the vascular endothelium (a monolayer of endothelial cells lining the inner lumen of all blood vessels) in preventing thrombosis, regulating the molecular exchange between blood and tissues, and administrating blood flow and vascular tone [50], we investigated the capability of (PEM/W2)₂ coating presented here as a coating of degradable Mg-stents to support HUVECs adhesion and proliferation. We established that endothelial cells adhered and grew on the base PEM film equally well as on TCP, considered the gold standard (Fig. 7). Composite (PEM/W2)₂ coating terminated with a thin wax layer suppressed HUVECs adhesion by about 13 % and proliferation by about 25 %. This is not surprising as a vast number of studies have shown that hydrophobic surfaces prevent protein adsorption and cell attachment, spreading and proliferation [51,52]. To combine the

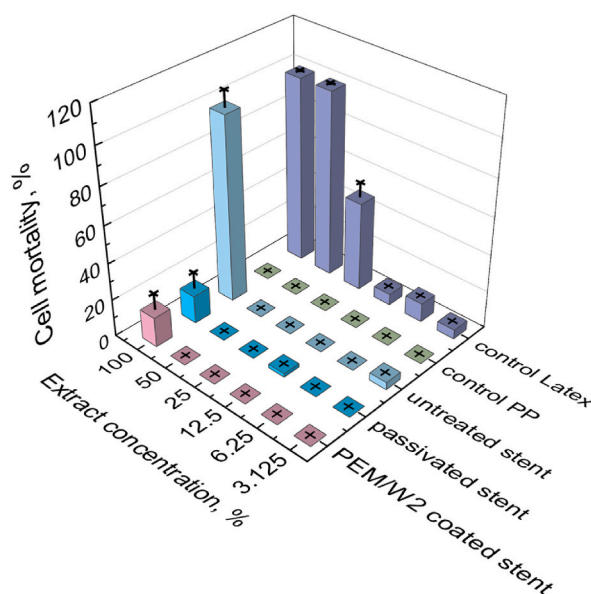


Fig. 6. *In-vitro* cell-growth inhibition of fibroblast L929 cells as a function of concentration of extraction medium from uncoated, passivated and (PEM/W2)₂ coated Mg-stents, as well as from positive control (latex) and negative control (polypropylene).

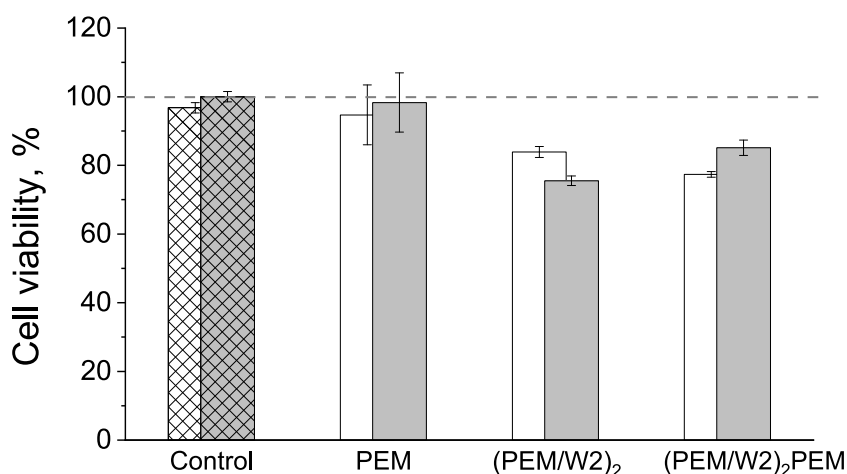


Fig. 7. HUVEC viability after 24 h of cultivation (white columns), demonstrating the extent of cell adhesion and after 72 h of cultivation (gray columns), demonstrating the extent of cell proliferation, examined on control TCP (hatched bars), PEM coating, PEM/W2 coating and PEM/W2/PEM coating.

proficiency of the (PEM/W2)₂ coating to retard the degradation of Mg-alloys with the cell-philic properties of PEM film, we constructed a (PEM/W2)₂PEM coating terminated with PEM. HUVECs displayed strong adhesion (80 % relative to the TCP control) and proliferation (85 % relative to the TCP control) on this composite coating (Fig. 7).

4. Conclusions

We have demonstrated that composite coatings combining polyelectrolyte multilayers and barrier wax layers possess an effective corrosion protection capacity and significantly reduce the degradation rate of coronary Mg stents. The coatings were built by layer-by-layer technology, employing three different types of wax-particles differing in surface charge, size and melting temperature. All wax particles contributed to the formation of coatings that appear smooth and homogeneous, without defects (surface openings), strongly adherent and completely covering the surface of the Mg-stent. The coating with the best anti-corrosion performance was very hydrophobic (contact angle 130°), and much thinner than all Mg-alloy coatings reported so far (only 210 nm). The *in-vitro* degradation tests proved that coated Mg-stents have greater resistance to degradation than uncoated and passivated ones. While after one week into the degradation medium, the uncoated and the passivated Mg-stents lost 2/3 of their scaffold volume, the coated Mg-stent, as well as the coating itself, appeared completely intact, with the whole integrity kept. Cytocompatibility studies demonstrated that Mg-stent coated with the composite PEM/Wax coating is not cytotoxic and improves the viability of fibroblast cells as compared to the uncoated Mg-stent.

Data availability statement

The authors confirm that the data supporting the findings of this study are available in the article and have been not deposited into a publicly available repository. Any additional raw data will be made available on request.

CRediT authorship contribution statement

Tonya D. Andreeva: Writing – original draft, Investigation, Data curation. **Oliver Walker:** Investigation, Data curation. **Alexander Rudt:** Investigation, Formal analysis. **Ole Jung:** Validation, Formal analysis. **Mike Barbeck:** Visualization, Investigation. **Manfred Gülcher:** Resources. **Rumen Krastev:** Supervision, Project administration, Funding acquisition, Conceptualization.

Declaration of competing interest

The all co-authors of the manuscript entitled “Composite polymer/wax coatings as a corrosion barrier of bioresorbable magnesium coronary stents” - Tonya Andreeva, Oliver Walker, Alexander Rudt, Ole Jung, Mike Barbeck, Manfred Gülcher, and Rumen Krastev declare that they have no conflict of interest.

We declare that the work described has not been published previously, that it is not under consideration for publication elsewhere, that its publication is approved by all authors and tacitly or explicitly by the responsible authorities where the work was carried out, and that, if accepted, it will not be published elsewhere in the same form, in English or in any other language, including electronically without the written consent of the copyright-holder.

Acknowledgments

The authors gratefully acknowledge the funding by the German Research Foundation (Deutsche Forschungsgemeinschaft, DFG) for the subproject 2 within the Research Unit 5250 “Permanent and bioresorbable implants with tailored functionality” (No. 449916462). The financial support of the German Federal Ministry of Education and Research (BMBF) within the project “BioDeg Stent” (Project Nr. FKZ 3FH155PX6) is also gratefully acknowledged.

References

- [1] E.P. Navarese, M. Kowalewski, D. Kandzari, A. Lansky, B. Górny, L. Koltowski, R. Waksman, S. Berti, G. Musumeci, U. Limbruno, R.J. van der Schaaf, M. Kelm, J. Kubica, H. Suryapranata, First-generation versus second-generation drug-eluting stents in current clinical practice: updated evidence from a comprehensive meta-analysis of randomised clinical trials comprising 31 379 patients, *Open Heart* 1 (2014) e000064, <https://doi.org/10.1136/openhrt-2014-000064>.
- [2] Y.H. Kim, A.Y. Her, S.W. Rha, B.G. Choi, S.Y. Choi, J.K. Byun, Y. Park, D.O. Kang, W.Y. Jang, W. Kim, J.Y. Baek, W.G. Choi, T.S. Kang, J. Ahn, S.-H. Park, J. Y. Park, M.-H. Lee, C.U. Choi, C.G. Park, H.S. Seo, Five-year clinical outcomes of first-generation versus second-generation drug-eluting stents following coronary chronic total occlusion intervention, *J. Geriatr. Cardiol.* 16 (8) (2019) 639–647, <https://doi.org/10.11909/j.issn.1671-5411.2019.08.006>.
- [3] B. Heublein, R. Rohde, V. Kaese, M. Niemeyer, W. Hartung, A. Haverich, Biocorrosion of magnesium alloys: a new principle in cardiovascular implant technology? *Heart* 89 (6) (2003) 651–656, <https://doi.org/10.1136/heart.89.6.651>.
- [4] H. Hornberger, S. Virtanen, A.R. Boccaccini, Biomedical coatings on magnesium alloys - a review, *Acta Biomater.* 8 (7) (2012) 2442–2455, <https://doi.org/10.1016/j.actbio.2012.04.012>.
- [5] X.N. Gu, Y.F. Zheng, Q.X. Lan, Y. Cheng, Z.X. Zhang, T.F. Xi, D.Y. Zhang, Surface modification of an Mg-1Ca alloy to slow down its biocorrosion by chitosan, *Biomed. Mater.* 4 (4) (2009) 044109, <https://doi.org/10.1088/1748-6041/4/4/044109>.
- [6] Y. Chen, Y. Song, S. Zhang, J. Li, C. Zhao, X. Zhang, Interaction between a high purity magnesium surface and PCL and PLA coatings during dynamic degradation, *Biomed. Mater.* 6 (2) (2011) 025005, <https://doi.org/10.1088/1748-6041/6/2/025005>.
- [7] H.M. Wong, K.W. Yeung, K.O. Lam, V. Tam, P.K. Chu, K.D. Luk, K.M. Cheung, A biodegradable polymer-based coating to control the performance of magnesium alloy orthopaedic implants, *Biomaterials* 31 (8) (2010) 2084–2096, <https://doi.org/10.1016/j.biomaterials.2009.11.111>.
- [8] J.E. Gray-Munro, C. Seguin, M. Strong, Influence of surface modification on the in vitro corrosion rate of magnesium alloy AZ31, *J. Biomed. Mater. Res. A* 91 (1) (2009) 221–230, <https://doi.org/10.1002/jbm.a.32205>.
- [9] J.N. Li, P. Cao, X.N. Zhang, Z.X. Zhang, Y.H. He, In vitro degradation and cell attachment of a PLGA coated biodegradable Mg–6Zn based alloy, *J. Mater. Sci.* 45 (2010) 6038–6045, <https://doi.org/10.1007/s10853-010-4688-9>.
- [10] W. Jiang, Q. Tian, T. Vuong, M. Shashaty, C. Gopez, T. Sanders, H. Liu, Comparison study on four biodegradable polymer coatings for controlling magnesium degradation and human endothelial cell adhesion and spreading, *ACS Biomater. Sci. Eng.* 3 (6) (2017) 936–950, <https://doi.org/10.1021/acsbomaterials.7b00215>.
- [11] L. Xu, A. Yamamoto, In vitro degradation of biodegradable polymer-coated magnesium under cell culture condition, *Appl. Surf. Sci.* 258 (17) (2012) 6353–6358, <https://doi.org/10.1016/j.apsusc.2012.03.036>.
- [12] G.A. Lakalaye, M. Rahvar, E. Haririan, R. Karimi, H. Ghanbari, Comparative study of different polymeric coatings for the next-generation magnesium-based biodegradable stents, *Artif. Cells, Nanomed. Biotechnol.* 46 (7) (2018) 1380–1389, <https://doi.org/10.1080/21691401.2017.1369424>.
- [13] K. Cai, X. Sui, Y. Hu, L. Zhao, M. Lai, Z. Luo, P. Liu, W. Yang, Fabrication of anticorrosive multilayer onto magnesium alloy substrates via spin-assisted layer-by-layer technique, *Mater. Sci. Eng. C* 31 (8) (2011) 1800–1808, <https://doi.org/10.1016/j.msec.2011.08.012>.
- [14] A. Mahapatro, L. Elson, R. Asmatulu, Formation of natural polyelectrolyte layer by layer (LBL) coating on magnesium alloy, *ECS Trans.* 53 (29) (2013) 21–27, <https://doi.org/10.1016/10.1149/05329.0021ecst>.
- [15] S. Kunjukunju, A. Roy, M. Ramanathan, B. Lee, J.E. Candiello, P.N. Kumta, A layer-by-layer approach to natural polymer-derived bioactive coatings on magnesium alloys, *Acta Biomater.* 9 (10) (2013) 8690–8703, <https://doi.org/10.1016/j.actbio.2013.05.013>.
- [16] N. Ostrowski, B. Lee, N. Enick, B. Carlson, S. Kunjukunju, A. Roy, P.N. Kumta, Corrosion protection and improved cytocompatibility of biodegradable polymeric layer-by-layer coatings on AZ31 magnesium alloys, *Acta Biomater.* 9 (10) (2013) 8704–8713, <https://doi.org/10.1016/j.actbio.2013.05.010>.
- [17] L.Y. Cui, R.C. Zeng, X.X. Zhu, Corrosion resistance of biodegradable polymeric layer-by-layer coatings on magnesium alloy AZ31, *Front. Mater. Sci.* 10 (2016) 134–146, <https://doi.org/10.1007/s11706-016-0332-1>.
- [18] L.-Y. Cui, S.-C. Cheng, L.-X. Liang, J.-C. Zhang, S.-Q. Li, Z.-L. Wang, R.-C. Zeng, In vitro corrosion resistance of layer-by-layer assembled polyacrylic acid multilayers induced Ca–P coating on magnesium alloy AZ31, *Bioact. Mater.* 5 (1) (2020) 153–163, <https://doi.org/10.1016/j.bioactmat.2020.02.001>.
- [19] P. Liu, X. Pan, W. Yang, K. Cai, Y. Chen, Improved anticorrosion of magnesium alloy via layer-by-layer self-assembly technique combined with micro-arc oxidation, *Mater. Lett.* 75 (2012) 118–121, <https://doi.org/10.1016/j.matlet.2012.02.016>.
- [20] F. Fan, C. Zhou, X. Wang, J. Szpunar, Layer-by-Layer assembly of a self-healing anticorrosion coating on magnesium alloys, *ACS Appl. Mater. Interfaces* 7 (49) (2015) 27271–27278, <https://doi.org/10.1021/acsami.5b08577>.
- [21] F. Gao, Y. Hu, G. Li, S. Liu, L. Quan, Z. Yang, Y. Wei, C. Pan, Layer-by-layer deposition of bioactive layers on magnesium alloy stent materials to improve corrosion resistance and biocompatibility, *Bioact. Mater.* 5 (3) (2020) 611–623, <https://doi.org/10.1021/acsami.5b08577>.
- [22] S. Borhani, S. Hassanajili, S.H.A. Tafti, S. Rabbani, Cardiovascular stents: overview, evolution, and next generation, *Prog. Biomater.* 7 (3) (2018) 175–205, <https://doi.org/10.1007/s40204-018-0097-y>.
- [23] E. Wittchow, N. Adden, J. Riedmüller, C. Savard, R. Waksman, M. Braune, Bioresorbable drug-eluting magnesium-alloy scaffold: design and feasibility in a porcine coronary model, *EuroIntervention* 8 (12) (2013) 1441–1450, <https://doi.org/10.4244/EIJV8I12A218>.
- [24] Y. Shi, L. Zhang, J. Chen, J. Zhang, F. Yuan, L. Shen, C. Chen, J. Pei, Z. Li, J. Tan, G. Yuan, In vitro and in vivo degradation of rapamycin-eluting Mg–Nd–Zn–Zr alloy stents in porcine coronary arteries, *Mater. Sci. Eng. C* 80 (2017) 1–6, <https://doi.org/10.1016/j.msec.2017.05.124>.
- [25] W. Xu, K. Sato, Y. Koga, M. Sasaki, T. Niidome, Corrosion resistance of HF-treated Mg alloy stent following balloon expansion and its improvement through biodegradable polymer coating, *J. Coating Technol. Res.* 17 (2020) 1023–1032, <https://doi.org/10.1007/s11998-019-00284-5>.
- [26] X. Gu, Z. Mao, S.-H. Ye, Y. Koo, Y. Yun, T.R. Tiasha, V. Shanov, W.R. Wagner, Biodegradable, elastomeric coatings with controlled anti-proliferative agent release for magnesium-based cardiovascular stents, *Colloids Surf., B* 144 (2016) 170–179, <https://doi.org/10.1016/j.colsurf.2016.03.086>.
- [27] J. Taavitsainen, S. Tarvainen, A. Kuivainen, E.K. Mangiardi, M. Guelcher, J. Martin, A. Mathur, J.P. Hytönen, S. Ylä-Herttua, Evaluation of biodegradable stent graft coatings in pig and rabbit models, *J. Vasc. Res.* 57 (2020) 65–75, <https://doi.org/10.1159/000505454>.
- [28] M.-H. Kang, K.-H. Cheon, K.-I. Jo, J.-H. Ahn, H.-E. Kim, H.-D. Jung, T.-S. Jang, An asymmetric surface coating strategy for improved corrosion resistance and vascular compatibility of magnesium alloy stents, *Mater. Des.* 196 (2020) 109182, <https://doi.org/10.1016/j.matdes.2020.109182>.
- [29] W. Xu, K. Yagoshi, T. Asakura, M. Sasaki, T. Niidome, Silk fibroin as a coating polymer for sirolimus-eluting magnesium alloy stents, *ACS Appl. Bio Mater.* 3 (2020) 531–538, <https://doi.org/10.1021/acsbm.9b00957>.
- [30] K. Glinel, M. Prevot, R. Krustev, G.B. Sukhorukov, A.M. Jonas, H. Möhwald, Control of the water permeability of polyelectrolyte multilayers by deposition of charged paraffin particles, *Langmuir* 20 (12) (2004) 4898–4902, <https://doi.org/10.1021/la036078l>.
- [31] P. Nazaran, V. Bosio, W. Jaeger, D.F. Anghel, R.v. Klitzing, Lateral mobility of polyelectrolyte chains in multilayers, *J. Phys. Chem. B* 111 (2007) 8572–8581, <https://doi.org/10.1021/jp068768e>.
- [32] J.A. Hiller, M.F. Rubner, Reversible molecular memory and pH-switchable swelling transitions in polyelectrolyte multilayers, *Macromolecules* 36 (2003) 4078–4083, <https://doi.org/10.1021/ma025837o>.

- [33] M. Alba, P. Formentín, J. Ferré-Borrull, J. Pallarès, L.F. Marsal, pH-responsive drug delivery system based on hollow silicon dioxide micropillars coated with polyelectrolyte multilayers, *Nanoscale Res. Lett.* 9 (1) (2014), <https://doi.org/10.1186/1556-276X-9-411> article number 411.
- [34] J.A. Lichter, M.F. Rubner, Polyelectrolyte multilayers with intrinsic antimicrobial functionality: the importance of mobile polycations, *Langmuir* 25 (2009) 7686–7694, <https://doi.org/10.1021/la900349c>.
- [35] A. Chassepot, L. Gao, I. Nguyen, A. Dochter, F. Fioretti, P. Menu, H. Kerdjoudj, C. Baehr, P. Schaaf, J.-C. Voegel, F. Boulmedais, B. Frisch, J. Ogier, Chemically detachable polyelectrolyte multilayer platform for cell sheet engineering, *Chem. Mater.* 24 (5) (2012) 930–937, <https://doi.org/10.1021/cm2024982>.
- [36] L. Mhamdi, C. Picart, C. Lagneau, A. Othmane, B. Grosgeat, N. Jaffrezic-Renault, L. Ponsonnet, Study of the polyelectrolyte multilayer thin films' properties and correlation with the behavior of the human gingival fibroblasts, *Mater. Sci. Eng. C* 26 (2006) 273–281, <https://doi.org/10.1016/j.msec.2005.10.049>.
- [37] C. Boura, P. Menu, E. Payan, C. Picart, J.-C. Voegel, S. Muller, J.-F. Stoltz, Endothelial cells grown on thin polyelectrolyte multilayered films: an evaluation of a new versatile surface modification, *Biomaterials* 24 (2003) 3521–3530, [https://doi.org/10.1016/s0142-9612\(03\)00214-x](https://doi.org/10.1016/s0142-9612(03)00214-x).
- [38] P. Tryoen-Toth, D. Vautier, Y. Haikel, J.-C. Voegel, P. Schaaf, J. Chluba, J. Ogier, Viability, adhesion, and bone phenotype of osteoblast-like cells on polyelectrolyte multilayer films, *J. Biomed. Mater. Res.* 60 (2002) 657–667, <https://doi.org/10.1002/jbm.10110>.
- [39] H. Kerdjoudj, N. Berthelemy, S. Rinckenbach, A. Kearney-Schwartz, K. Montagne, P. Schaaf, P. Lacolley, J.F. Stoltz, J.-C. Voegel, P. Menu, Small vessel replacement by human umbilical arteries with polyelectrolyte film-treated arteries: in vivo behavior, *J. Am. Coll. Cardiol.* 52 (2008) 1589–1597, <https://doi.org/10.1016/j.jacc.2008.08.009>.
- [40] K. Glinel, M. Prevot, R. Krustev, G.B. Sukhorukov, A.M. Jonas, H. Möhwald, Control of the water permeability of polyelectrolyte multilayers by deposition of charged paraffin particles, *Langmuir* 20 (2004) 4898–4902, <https://doi.org/10.1021/la036078l>.
- [41] M. Elźbięciak-Wodka, P. Warszyński, Effect of deposition conditions on thickness and permeability of the multilayer films formed from natural polyelectrolytes, *Electrochim. Acta* 104 (2013) 348–357, <https://doi.org/10.1016/j.electacta.2012.10.169>.
- [42] S. Lebrette, C. Pagnoux, P. Abélard, Stability of aqueous TiO₂ suspensions: influence of ethanol, *J. Colloid Interface Sci.* 280 (2) (2004) 400–408, <https://doi.org/10.1016/j.jcis.2004.07.033>.
- [43] X. Liu, S. Tang, H.K. Choi, H.S. Choi, Effect of plasma-treated polymer substrates on fabricating surface microsystems through LbL coating, *Macromol. Res.* 18 (2010) 413–420, <https://doi.org/10.1007/s13233-010-0506-0>.
- [44] Y. Xin, T. Hu, P.K. Chu, Influence of test solutions on in vitro studies of biomedical magnesium alloys, *J. Electrochem. Soc.* 157 (2010) C238–C243, <https://doi.org/10.1149/1.3421651>.
- [45] E.L. Boland, J.A. Grogan, P.E. McHugh, Computational modelling of magnesium stent mechanical performance in a remodelling artery: effects of multiple remodelling stimuli, *Int. J. Numer. Method. Biomed. Eng.* 35 (10) (2019) e3247.
- [46] G.L. Song, A. Atrens, Corrosion mechanisms of magnesium alloys, *Adv. Eng. Mater.* 1 (1) (1999) 11–33.
- [47] J.J. Harris, P.M. DeRose, M.L. Bruening, Synthesis of passivating, nylon-like coatings through cross-linking of ultrathin polyelectrolyte films, *J. Am. Chem. Soc.* 121 (9) (1999) 1978, <https://doi.org/10.1021/ja9833467>.
- [48] A.H.M. Sanchez, B.J.C. Luthringer, F. Feyerabend, R. Willumeit, Mg and Mg alloys: how comparable are in vitro and in vivo corrosion rates? A review, *Acta Biomater.* 13 (2015) 16–31, <https://doi.org/10.1016/j.actbio.2014.11.048>.
- [49] N.A. Agha, F. Feyerabend, B. Mihailova, S. Heidrich, U. Bismayer, R. Willumeit-Römer, Magnesium degradation influenced by buffering salts in concentrations typical of in vitro and in vivo models, *Mater. Sci. Eng. C* 58 (2016) 817–825, <https://doi.org/10.1016/j.msec.2015.09.067>.
- [50] Y. Matsuzawa, A. Lerman, Endothelial dysfunction and coronary artery disease: assessment, prognosis, and treatment, *Coron. Artery Dis.* 25 (8) (2014) 713–724, <https://doi.org/10.1097/MCA.0000000000000178>.
- [51] T. Ishizaki, N. Saito, O. Takai, Correlation of cell adhesive behaviors on superhydrophobic, superhydrophilic, and micropatterned superhydrophobic/superhydrophilic surfaces to their surface chemistry, *Langmuir* 26 (2010) 8147–8154, <https://doi.org/10.1021/la904447c>.
- [52] M. Carmen Morán, G. Ruano, F. Cirisano, M. Ferrari, Mammalian cell viability on hydrophobic and superhydrophobic fabrics, *Mater. Sci. Eng. C* 99 (2019) 241–247, <https://doi.org/10.1016/j.msec.2019.01.088>.